Chemical Engineering Research and Design 227 (2026) 223–233

Contents lists available at ScienceDirect

Chemical Engineering Research and Design

journal homepage: www.elsevier.com/locate/cherd

Numerical study of multiphase mixing of micron sized aggregates in opposed jets fluidized bed

Muhammad Usman Farid [a,*], Laura Unger [b], Dyrney Araújo dos Santos [c], Andreas Bück [a]

[a] Thermal Process Engineering, Otto von Guericke University Magdeburg, Universitätsplatz 2, Magdeburg D-39106, Germany
[b] Interfaces and Particle Technology, Friedrich-Alexander University Erlangen-Nuremberg, Cauerstr. 4, Erlangen D-91058, Germany
[c] Institute of Chemistry, Federal University of Goiás - UFG, Campus Samambaia, Goiânia, GO 74690-900, Brazil

ARTICLE INFO

Keywords:
CFD
Multiphase flow
Fluidized bed
Mixing
Cohesive particles

ABSTRACT

Fine aggregates are considered as essential elements in the production of a wide range of food, pharmaceutical as well as other chemical products. In process industry, mixing of such particles is a crucial operation which controls the quality, texture and attributes of the final product. However, mixing becomes quite challenging while dealing with cohesive particles because of strong inter particulate forces, mostly van der Waals or capillary forces. A strong external force is required to overcome the cohesive forces and eventually, to agitate and mix such aggregates. With several advantages, mixing of such aggregates can be carried out in gas phase regime using fluidized bed systems. However, gas-solid environment yields to turbulence multiphase flow dynamics which needs to be investigated for optimum performance. In the current study, a two-way coupled Euler-Lagrange CFD model has been developed for the investigation of hydrodynamics and mixing of multiphase flows in an opposed jets fluidized bed. In total two phases were selected including air as a gas phase whereas TiO_2 was considered as the solid phase. Particles were placed in the domain at known quantity and different streams of air jet were injected with the help of three nozzles mounted in the bottom and side walls of the apparatus. As a result, fluid dynamically different zones were formed such as stressing zone and mixing zone. Increasing air flow rate, the suspension and mixing of particles is improved. However, very high air injections results in formation of wall bounded layer of particles which negatively effects the mixing. High particle concentration was found near the wall in case of air flow rate injected at a flow rate of 0.003 kg/s. Further investigations are planned in order to further explore effect of dynamic classifier, particle size distribution and mass loading.

1. Introduction

Fine aggregates are considered as an essential element in production of a wide range of food, pharmaceutical, construction as well as chemical products. With typical particle size less than 50 µm, such fine powders have gained significant industrial attraction because of their increased surface area (Ghoroi et al., 2013; Peukert and Bück, 2024). In process industry, mixing and dispersion of such particles is a crucial operation which controls the quality, texture and attributes of the final product. For instance, homogeneity is one of the critical parameters, particularly, in sensitive applications such as pharmaceutical products, where a slight deviation may result in product failure (Salloum et al., 2025). Similarly, formulation of hetero-aggregates also depends on effective mixing and blending of different homo-aggregates (Men et al., 2023). However, mixing becomes quite challenging while dealing with micron sized dry cohesive particles. Because of strong interparticle forces mostly van der Waals or capillary forces, it becomes very hard to fluidize such particles (Jadidi et al., 2025). A strong external force is required to overcome such cohesive forces and hence, to affectively mix the aggregates. Furthermore, flow behaviour of such aggregates significantly affects the equipment hydrodynamics (Lepek et al., 2010; Thomas, 2025).

Generally, mixing of aggregates can be carried out through liquid phase and gas phase processes. The former approach involves dispersions of oppositely charged colloids and mixing in liquid form. The mixture is, eventually, transformed to fine powders upon drying. In this way, the composition of resulting fine aggregates can be customized by controlling the charge and mass fraction of colloids during the liquid dispersion (Kolan et al., 2024; Men et al., 2023). However, this method faces several challenges such as solvents incompatibility, stability of

* Corresponding author.
E-mail address: muhammad1.farid@ovgu.de (M.U. Farid).

https://doi.org/10.1016/j.cherd.2026.01.056
Received 30 October 2025; Received in revised form 12 January 2026; Accepted 26 January 2026
Available online 27 January 2026

aggregates, sedimentation, contamination, separation from by-product etc. On the other hand, gas phase process offers more energy efficient and operational benefits through flame spray pyrolysis, electro-spray pyrolysis and dry formulation techniques. Amongst, the dry formulation has been recognized as one of the simplest, cost-effective and eco-friendly methods for mixing of cohesive fine aggregates. In this technique, the fine powders are agitated intensely with the help of high-speed gas jet to form homogeneous final product. However, having very high surface area to volume ratios and strong cohesive forces, mixing and blending of fine aggregates is quite challenging process. An external force, in the form of high gas flow, is required to overcome these interparticle forces and eventually to fluidize such particles (Men et al., 2023; Nascimento et al., 2025).

When it comes to controlled mixing, utilization of fluidized bed apparatus holds several merits. For instance, fluidized beds offer excellent contact between multiphase systems, e.g., solid particles and gas stream. Consequently, this process enhances mixing and mass transfer within the system, resulting in improved homogeneity and uniformity of the produced aggregate (Gao et al., 2020). Because of this unique feature, such kind of apparatuses are widely being used for mixing and agglomeration of different product in process industry (Ali and Asif, 2017; Tashakori-Asfestani et al., 2023; Van Ommen et al., 2012). However, optimization of process parameters is required in case of cohesive particles in order to ensure process efficiency and optimal operational cost (Sharma et al., 2025).

Mixing of fine aggregates using fluidized bed systems have been explored by several researchers. For example, Liu and Wang (2021) studied the behaviour of SiO_2 particles agglomeration under variable bed hight and found that with a high particles bed, it is very difficult to reach steady state conditions because of strong cohesive forces. Quevedo et al. (2010) investigated different metal oxide particles agglomeration using microjets and concluded that the particle motion is significantly improved with the help of microjets and hence, blending of different particles can be achieved at nanoscale. Koeninger et al. (2018a) studied the milling of glass beads in an opposed jets fluidized bed and found that the internal recirculation and particle accumulation in the mill classifier is crucial which should be further deeply investigated. Similarly, Strobel et al. (2020) investigated the stress conditions in the opposed jets fluidized bed and concluded that the stressing inside the jet mill is a result of multiple collisions caused by recirculation. In both studies grinding and milling of particles was focused with a particle size greater than 50 μm. A further fine aggregates may function differently using such apparatus which needs further in depth investigations. Men et al. (2023) explored the potential of fluidization technologies for the formulation of fine hetero-aggregates. Based on the experimental investigations, they found that the spouted bed faces initial difficulties to achieve fluidization because of interparticle forces whereas intense mixing without major hindrance can be obtained in case of opposed jets fluidized bed. Similarly, Kolan et al. (2024) studied the nanoparticle mixing in a ProCell spouted bed to produce hetero-aggregates at high jet velocities. They found that increasing jet velocity improves the dispersion, however, at too high inlet velocity elutriation becomes dominant. Recently, Nascimento et al. (2025) from our group reported an experimental study on the formulation of hetero-aggregates in the opposed jets fluidized bed in which different combination of primary particles (TiO_2 and ZrO_2) were employed to formulate hetero-aggregates. The overall findings endorsed that the opposed jets fluidized bed can be effectively used for the formulation of highly porous aggregates having morphological attributes similar to the primary particles. However, the process parameters have a significant effect on the aggregate-contacts, shape factors as well as dimensions of the produced aggregates and hence, this propels in-depth analyses and optimization of the process involved in particle mixing and agglomeration within the apparatus.

Application of external force in terms of high-speed gas jets results in turbulent flows leading to high momentum transfer among fluid to particle and particle to particle interactions. Hence, understanding the internal hydrodynamics of the apparatus is crucial for the optimum performance. Computational fluid dynamics (CFD) has been identified as a useful tool for the process simulation of multiphase systems up to industrial scale (Chen et al., 2019; Lince et al., 2011; Lu et al., 2025). Generally, two methods are employed for the investigation of fluid-particle systems, the Eulerian-Eulerian approach and Eulerian-Lagrangian approach. The former approach considers all phases as interpenetrating continua while the latter approach treats the primary (fluid) phase in the Eulerian frame of reference whereas particles are tracked individually as a discrete phase. Application of either technique depends on the type of process and the configuration of the apparatus (Unger et al., 2022). Moreover, adoption of multiphase models for the simulation of high-speed jet mixing of particulate system requires particular attention as multiple boundary conditions needs to be applied as a realistic approach. Efforts to implement of CFD modelling approach to simulate the opposed jets fluidized bed mills has been reported by few researchers. For example, Rajeswari et al. (2011) studied numerical simulation of opposed jets fluidized bed mill by using the Eulerian multiphase model. Primary phase (air) was injected through the bottom nozzles whereas secondary phase (silica particles) was injected from the top inlet (without transport air). Although a good agreement was established in a comparison of mass balance, further investigation to improve model and realistic boundary conditions were recommended. Another study was reported by Santos et al. (2020) in which opposed jets fluidized bed was simulated for mixing of glass microspheres (55 μm) under Euler-Euler approach. The particle flow as well as the concentration under variable conditions were simulated and compared with the experimental results. It was concluded that particle interaction and resulting momentum is not only because of air jets but also influenced by the apparatus walls in the grinding zone as well as classification zone. Similarly, Lee et al. (2019) numerically investigated air jet mill for the grinding of ceramic particles with the help of CFD-DEM approach. Huang et al. (2024) studied CFD simulation of the flow field in a steam fluidized bed jet mill. They found that there is significant fluctuation in the flow field due to presence of secondary phase, hence, effects the overall grinding efficiency. Although notable contributions have been made by the researchers, numerical simulation of opposed jets fluidized bed is still challenging to describe the actual process.

In the current study, a two-way coupled Euler-Lagrange CFD model has been developed for the investigation of hydrodynamics and mixing of multiphase flows in an opposed jets fluidized bed. The focus of this study was to understand internal hydrodynamics, mixing behaviour and regions of high particle suspension inside the apparatus. The novelty of the present study lies in the use of fully three-dimensional Euler–Lagrange (CFD–DEM) simulations to resolve particle-scale dynamics in an opposed jets fluidized bed. While most numerical studies rely on the Euler–Euler approach due to its lower computational cost, this framework cannot accurately capture particle–particle interactions and detailed mixing mechanisms. Only a limited number of studies have applied Euler–Lagrange methods to such systems, and existing simulations (e.g., Santos et al., 2020) are mainly two-dimensional and based on Euler–Euler formulations. Our simulations provide new mechanistic insights into the internal hydrodynamics, including (i) the origin of fluid recirculation and vortex formation in the stressing zone due to jet interaction, (ii) the role of gas flow rate in enhancing particle kinetic energy and dispersion, and (iii) the adverse effect of excessively high jet velocities, which drive particles toward the walls and reduce effective interaction in the upper mixing region. These findings go beyond reproducing experimental trends and contribute to a fundamental understanding of multiphase flow and mixing in opposed jets fluidized beds.

The manuscript is structured as: Section 2 provides the methodology adopted in this work, the insights and description of results are given in Section 3, while Section 4 presents the major conclusion and provides an outlook on future work.

2. Methodology

2.1. Process setup: Opposed jets fluidized bed

The process under consideration is mixing of micron sized homo-aggregates in an opposed jets fluidized bed (AFG 100, Hosokawa Alpine, Germany). This equipment is commonly used on industrial scale for comminution and mixing of bulk solids. Fig. 1 presents the components and working principle of this apparatus. The fluidized bed consists of major components as: stressing zone and mixing zone. In the beginning, the feed material (homo-aggregates) is introduced at the bottom of the fluidized bed. High speed air is injected via three Laval nozzles, i.e., the central nozzle is mounted in the bottom while the other two nozzles are installed in the side walls of the fluidized bed (Nascimento et al., 2025). The both nozzles are inclined with an angle of 30° forming an opposite jet stream as shown in Fig. 1. The nozzles have an outlet diameter of 2.4 mm whereas the dimeter at the contraction is 1.9 mm (Hosokawa-Alpine AFG 100).

The air injected at high speed helps to agitate the homo-aggregates by overcoming the interparticulate (van der Waals) forces. The central jet helps to fluidize the particles in the form of a spout whereas the side jets contribute to an intense stressing and rapid mixing of the particles. The feed material is further accelerated by the air stream flowing and transporting through the mixing zone. A rotating classifier is installed at the upper region of the apparatus forming a classification section to separate the final product from air. To simplify the geometry of the computational model, the classifier is not considered. Further details and experimental description of the process can be found in Men et al. (2023).

2.2. Numerical simulation approach

A 3D model of the fluidized bed shown in Fig. 1 was designed using the Design Modeler available in ANSYS Workbench (V 2024 R2). The geometry (Fig. 2) was converted into a computational domain (mesh) using Fluent Meshing Tool which is an integrated meshing platform. The structured meshing approach was used to generate a poly-hexcore mesh consisting of 0.44 million cells and 2 million faces (Fig. 2). The poly-hexcore mesh consists of a combination of hexahedral and polyhedral cells as well as prismatic boundary layers which provides superior features to increase quality and accuracy, especially in case of complex geometries and high turbulent flows (Sudsuansee et al., 2025; Wróblewski et al., 2024). Exposed to high-speed flows and resulting in

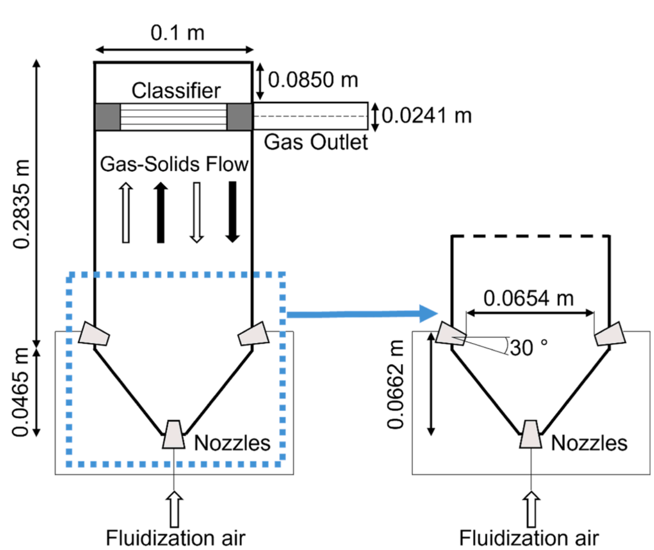

Fig. 1. Schematic illustration of the opposed jets fluidized bed (adapted from (Santos et al., 2020; Men et al., 2023)).

higher degree momentum, the inlet and outlet points and the bottom part of the apparatus, i.e., stressing zone was refined enabling a minimum orthogonal quality of 0.78.

A two-way coupled CFD model based on the Euler-Lagrange approach was adopted using ANSYS-Fluent (V 2024 R2). Air was considered as primary/continuous phase whereas TiO_2 homo-aggregates particles were considered as discrete phase (Table 1). As very high circulating flow is expected, the k-ω (SST) model was used for the modelling of fluid flow and turbulence (Farid et al., 2017; Farid et al., 2025). The transport equation of this model is based on two variables, i.e., the turbulence kinetic energy (k) and the specific rate of dissipation (ω) which are solved for (Fluent, 2022; Farid et al., 2017; Menter et al., 2003):

$$\frac{\partial}{\partial t}(\rho_g k) + \frac{\partial}{\partial x_i}(\rho_g k u_i) = \frac{\partial}{\partial x_j}(\Gamma_k \frac{\partial k}{\partial x_j}) + G_k - Y_k + S_k \tag{1}$$

$$\frac{\partial}{\partial t}(\rho_g \omega) + \frac{\partial}{\partial x_i}(\rho_g \omega u_i) = \frac{\partial}{\partial x_j}(\Gamma_\omega \frac{\partial \omega}{\partial x_j}) + G_\omega - Y_\omega + S_\omega \tag{2}$$

where G represents the generation term, Γ is the effective diffusivity, Y represents dissipation due to turbulence, and S represents the defined source term. The subscripts k and ω represent respective terms for the turbulence kinetic energy (k) and the specific rate of dissipation of turbulence kinetic energy (ω).

The Discrete Phase Model (DPM) was used for particle tracking with unsteady particle treatment which considers changing interaction between continuous phase and the TiO_2 particles over time. The DPM in ANSYS (Fluent) is based on Euler-Lagrange approach (Fluent, 2022; Farid et al., 2025):

$$m_p \frac{d\overrightarrow{u_p}}{dt} = m_p \frac{18\mu_f}{\rho_p\, d_p^2} \frac{C_d \mathrm{Re}}{24} (\overrightarrow{u_f} - \overrightarrow{u_p}) + m_p \frac{g(\rho_p - \rho_f)}{\rho_p} + \overrightarrow{F_s} \tag{3}$$

where m_p, u_p, d_p and ρ_p represent mass, velocity, diameter and density of the discrete phase (particles), respectively whereas u_f is the fluid velocity, ρ_f is the fluid density, μ_f is the fluid viscosity, C_d is drag coefficient and F_s denotes the external body forces.

The Stokes-Cunningham Model was used to consider the drag force (F_D) as (Fluent, 2022):

$$F_D(u_f - u_p) = \frac{\mu_f}{\rho_p d_p^2} \frac{18 C_d \mathrm{Re}}{24} (u_f - u_p) \tag{4}$$

Where the drag coefficient (C_d) is computed as (Fluent, 2022):

$$C_d = \frac{24}{\mathrm{Re}_p C_c} \tag{5}$$

where Re_p is the particle Reynolds number and C_c is the Conningham correction to the drag law computed internally by the fluent by each particle with respect to each tracking step.

The opposite jets cause rotational movement of particles eventually leading to higher rotational Reynolds number. Hence, rotational drags law was also enabled which uses the following correlation proposed by Dennis et al. (Dennis et al., 1980; Fluent, 2022) to compute rotational drags law coefficient (C_ω):

$$C_\omega = \frac{6.45}{\sqrt{\mathrm{Re}_\omega}} + \frac{32.1}{\mathrm{Re}_\omega} \tag{6}$$

$$\mathrm{Re}_\omega = \frac{\rho_f \left|\overrightarrow{\Omega}\right| d_p^2}{4\mu_f} \tag{7}$$

where Re_ω is rotational Reynolds number. The angular velocity is computed for each particle with help of angular momentum equation (Fluent, 2022):

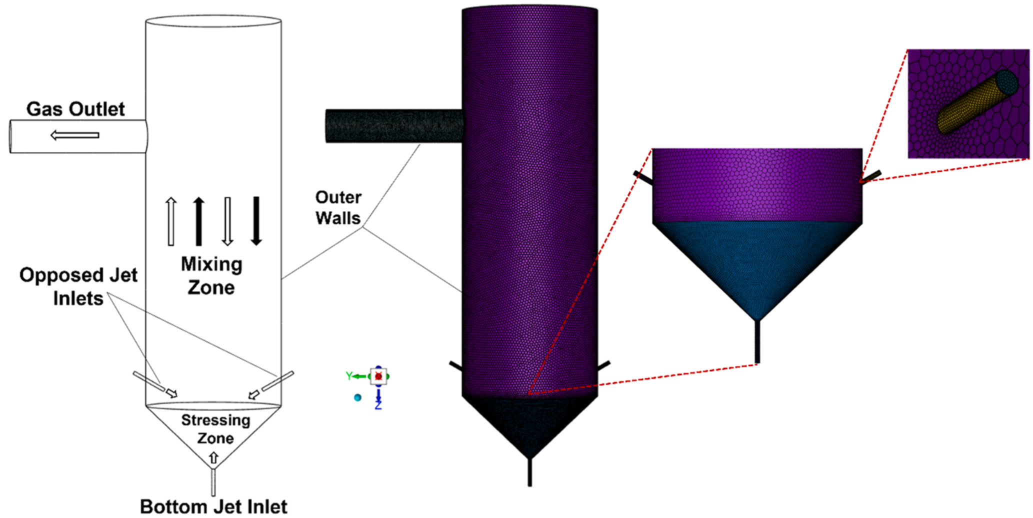

Fig. 2. Computational domain and generated mesh for the opposed jets fluidized bed.

Table 1
Models and Boundary Conditions.

CFD Approach	Model	Settings/Value
Computational Mesh	Structured (3D) Poly-hexcore	Number of Cells = 435795 Min Orthogonal Quality = 0.78
Turbulence and Fluid Flow	k-omega (SST) Model	Model Constants = Default Settings
Multiphase Approach DPM Model (Two-Way Coupled)	Eulerian-Lagrange Approach Unsteady Particle Treatment Particle Type and Count Momentum Exchange Tracking Steps Particle Dispersion	Primary Phase = Air Secondary Phase = TiO_2 Particles Particle Time Step Size = 0.001 s, DPM Interaction = 10 Flow Iterations Inert, 20000 Particles (Parcels), Particle Size Distribution = Uniform Drag Law = Stokes-Cunningham Model Particle Rotation = Dennis et al. Model Lift Law = Rubinow-Keller Model 5000 Discrete Random Walk Model (Time Scale Constant = 0.15)
Modeller/Scheme Solver Pressure Scheme Solution Initialization	Steady-State Pressure-Velocity Coupling Pressure	10000 Iterations Pressure-Based Coupled Pressure Staggering Option Hybrid
Inlet Gas Flowrate		Case 1 = 0.001 kg/s Case 2 = 0.002 kg/s Case 3 = 0.003 kg/s
Particle Size		1 μm
Particle Size Distribution		Monodisperse
Particle Density		3900 kg/m^3
Total Mass in Batch		10 g
Boundary Conditions	Inlet	Mass Flow Inlet (uniform in all inlets)
	Outlet	Pressure Outlet, Particle Flow Restricted
	Walls	No Slip, Stationary Walls (Fig. 2)

$$I_P \frac{d\overrightarrow{\omega_p}}{dt} = \frac{\rho_f}{2}\left(\frac{d_p}{2}\right)^5 C_\omega \left|\overrightarrow{\Omega}\right| . \overrightarrow{\Omega} = \overrightarrow{T} \tag{8}$$

where, I_P is moment of inertia, ω_p is annular velocity of particles, $\overrightarrow{T}$ is the torque applied to the particle and $\overrightarrow{\Omega}$ is the relative fluid-particle angular velocity determined as $0.5\nabla\left(\overrightarrow{u_f} - \overrightarrow{\omega_p}\right)$.

Similarly, rotational lift force (F_r) also termed as Magnus effect, was included which is governed by the rotational lift force coefficient (C_r) as (Fluent, 2022):

$$F_r = 0.5 A_p C_r \rho_f \frac{\left|\overrightarrow{V}\right|}{\left|\overrightarrow{\Omega}\right|}\left(\overrightarrow{V}\overrightarrow{\Omega}\right) \tag{9}$$

where A_p is the surface area of projected particles, $\overrightarrow{V}$ and $\overrightarrow{\Omega}$ are the relative fluid-particle velocity and angular velocity, respectively. Several approaches are used to determine the rotational lift force coefficient (C_r). In the current study, the Rubinow-Keller model was adopted which is based on the assumption that C_r is linearly proportional to the spin factor S as

$$C_r = 2S \tag{10}$$

where spin factor S is determined as (Fluent, 2022):

$$S = \frac{\left|\overrightarrow{\omega_p}\right| d_p}{2\left|\overrightarrow{u_f} - \overrightarrow{u_p}\right|} \tag{11}$$

The Discrete Random Walk model was included to consider the effect of turbulence on particle motion and its dispersion with a time scale constant (C_L) of 0.15 (Fluent, 2022; Farid et al., 2017).

Table 1 summarizes the model settings and boundary conditions used in the current work. A two-way coupled steady state (continuous phase) simulation scheme was adopted with 10000 iterations. However, unsteady particle treatment was considered with particle time step size of 0.001 s and DPM iteration interval of 10. Under this approach, the fluid phase is considered as quasi-steady. However, the momentum exchange between continuous (fluid) phase and the particles is computed during the particle tracking which is then iteratively incorporated as source term in the steady state flow field. Moreover, the particle-particle collisions were not taken into consideration the current settings. The primary goal was to study the dynamic behaviour of micron sized particles under variable jet injections. For this purpose, micron sized TiO_2 particles were taken as test material for the current simulations. The simulation was initialized with 20000 TiO_2 homo-aggregates (parcels) having uniform size (1 μm) which were placed in the bottom of the fluidized bed comprising a total mass of one batch as 10 g which is in line with experiments of Men et al. (2023) and Nascimento et al. (2025). The 'coupled' pressure-velocity numerical approach was adopted with pressure discretization scheme 'Presto!'. All simulations were performed using a Windows-based system with Intel Core i9 CPU (3.30 GHz) and 64 GB of RAM. The numerical setup was used to investigate the effect of variable jet injection rates on particle dynamics and recirculation within the apparatus which was indicated as one of the most important variables according to Men et al. (2023) and Nascimento et al. (2025). For this purpose, three cases were studied, i.e., Case 1 (0.001 kg/s), Case 2 (0.002 kg/s) and Case 3 (0.003 kg/s). The flow injection lies in turbulence flow regime, i.e., Re > 28,000.

3. Results and discussion

The set of numerical simulations were conducted for different cases of gas inlet mass flow rates. The different jet injections resulted in different hydrodynamics fields in the apparatus significantly impacting the particle mixing in the apparatus domain. The effect of gas injection rate on the flow field as well as particle flow has been discussed as below.

3.1. Grid independence verification

In order to evaluate the influence of grid size on numerical solution, three computational domains of different mesh sizes were formulated. The mesh M1 was taken as a fundamental coarse mesh consisting of 0.22 million elements with uniform mesh size of the whole apparatus. In case of M2, the bottom part of the domain was refined to form a total of 0.44 million cells which is double in number as compared to M1. Similarly, M2 was further refined to form a fine mesh M3 with 0.95 million cells as shown in Fig. 3. For the verification of the three mesh domains, the flow field at the stressing zone, being the most critical part of such kind of fluidized beds, was studied with same numerical setup and operating conditions (Case 1). For this purpose, a flow profile along the axial direction within the apparatus was extracted and compared among the different meshes. All cases of mesh sizes showed qualitatively similar flow trend. For example, the flow field gradually increases while moving from wall towards the center of the apparatus and a velocity peak is found at a distance of 20 mm from the side wall. This typical formation is result of the high-speed gas jet coming from the side nozzle (as illustrated in Fig. 1). The flow at the center is reduced indicating a low-speed region created by diffusion of both flow vertices (Fig. 4). Afterwards, the second flow peak is found caused by the second nozzle mounted at the opposite side wall. Comparison showed that the peak flow velocity was 65 m/s in case of coarse mesh (M1) whereas the M2 and M3 meshes showed quite similar peak values, i.e., 85 and 87 m/s, respectively. Moreover, it can also be observed that as number of cells increase, a more consistent flow field is obtained throughout the axial length. Having similar flow trends as well as peak velocities, it can be speculated that refining mesh size beyond M2 has a minor effect on the numerical solution. Moreover, the flux report also indicated that M2 has the least relative error, i.e., 0.0019 % among the three different mesh sizes. Hence, the mesh M2 was adopted for further investigations in this study.

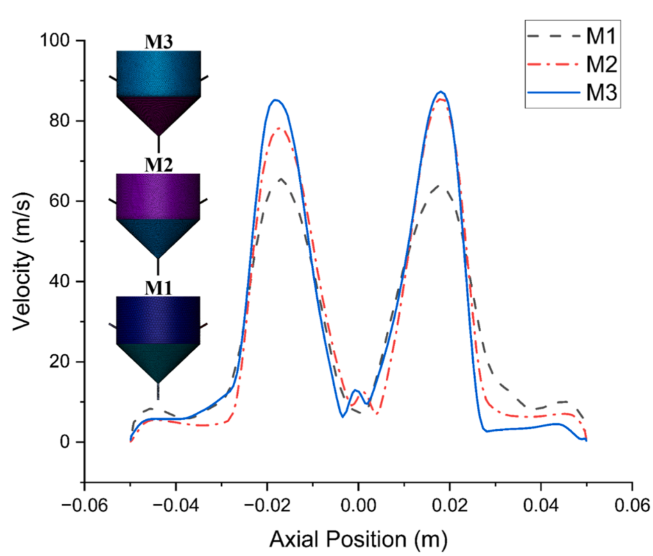

Fig. 3. Comparison of axial flow field with different mesh sizes.

3.2. Effect of injection rate on flow field

The flow field in the stressing zone is of prime importance as it helps to initially accelerate the particles which contributes in overall mixing performance. The numerical result in Fig. 4 shows that the air jet supplied through the nozzles enters the apparatus domain in the form of a high-speed stream, i.e., a maximum velocity of 190 m/s can be observed in Case 1. Having similar flow pattern through all the inlets, the three jet streams meet in the centre of the stressing zone. Moreover, it can also be observed that the opposed jet inlets produce a counter flow pattern leading to formation of recirculating flow vertices in the domain. In this way, the bottom jet lifts up the particles (initially at rest) to form a spout (same as spouted bed). The flow produced by the counter jets helps to collide and potentially starts the fluidization of the homo-aggregates with the help of strong flow vertices in the stressing zone (Fig. 4). A similar trend has also been observed in the previous study reported by Rajeswari et al. (2011).

Fig. 5 illustrates the flow field and velocity vector for an injection flowrate of 0.002 kg/s (Case 2). By increasing the air flow rate, the bottom jet experiences a strong counter flow created by the opposed jet nozzles. Due to this effect, the flow pattern is restricted and deviated which was more organized towards the centre in Case 1. However, this effect improves the vertices formation in the stressing zone which helps to more rapidly mix the particles. Similar behaviour was also observed in case of an injection flow rate of 0.003 kg/s (Case 3, Fig. 6). Having significantly higher velocity of air, the deviation of bottom jet occurs at the jet intersecting zone as compared to Case 2. However, the flow vertices have similar pattern in both cases. To further analyse this effect, a set of dynamic simulation was also carried out. The results indicated that initially the bottom jet experiences a high resistance because of the particles placed in the bottom part. After excited by high gas flow rate, the particles are lifted up which are then recirculated by the opposite jet streams. After mixing in the stressing zone, the particles are transported to the upper region of the apparatus. The steady state conditions showed that the deflection of bottom jet is mainly caused by the opposite jets.

After the stressing zone, the velocity of the flow field is decreased which is because of dispersion induced decay as also observed by Huang et al. (2024) and Rajeswari et al. (2011). However, a significant variation in the local velocities is observed in the transport region. This phenomenon improves the interaction between particle and fluid and promotes mixing behaviour. In order to analyse and compare the velocity profile of the flow field, the domain was divided into six planes throughout the fluidized bed: Plane 1 is located in the centre of the stressing zone, i.e., at a height (h) of 0.02 m from the bottom. Plane 2 is located at height of 0.05 m and represents the top of the stressing zone. Plane 3 indicates the region beneath the injection point of the opposed jet inlets having a vertical position of 0.06 m from the bottom, Plane 4 is located at a vertical height of 0.15 m, i.e., forming the centre of the mixing zone, Plane 5 shows the area in the middle of outlet pipe positioned at a height of 0.25 m and Plane 6 is located at a height of 0.29 m from bottom of the apparatus.

Fig. 7 compares the flow field among the three cases of air flow rates

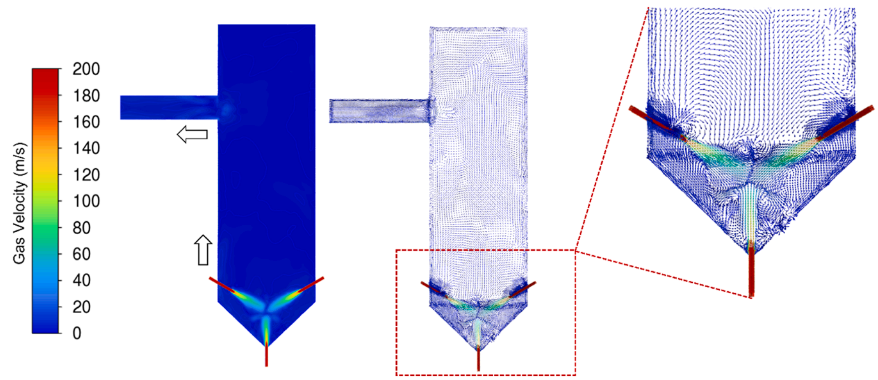

Fig. 4. Velocity profile of air **(Case 1)**.

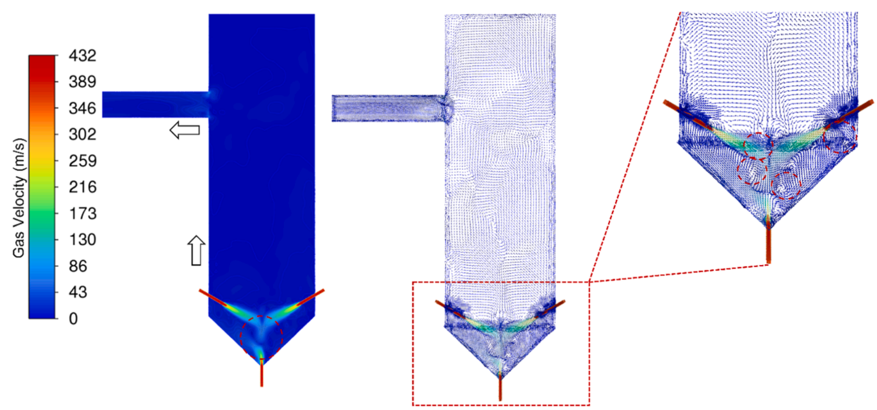

Fig. 5. Velocity profile of air **(Case 2)**.

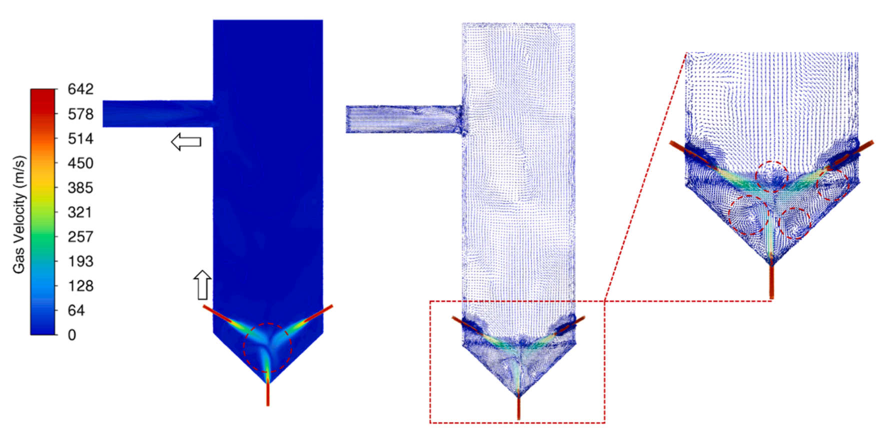

Fig. 6. Velocity profile of air **(Case 3)**.

at Plane 1. It can be observed that Case 1 results in more homogenous flow pattern whereas strong vertices in the flow field are generated in Case 2 and Case 3. Moreover, the circular spot in Fig. 7 indicates the velocity of central (bottom nozzle) where the elongated flow pattern is generated as a result of deflection of bottom jet and the counter jets. As a result, the jet stream flows along the apparatus wall and then mixed again in the centre, forming the flow vertices as shown in Fig. 8. Similar trend has been observed by Huang et al. (2024) where the organized pattern of the flow field translates to more vortices by increasing the injection mass flow rate.

The recirculation vertices at the stressing zone are prominently built up with high entrainment of gas into the apparatus (Fig. 6 and Fig. 8) which has a similar trend as observed by Santos et al. (2020). Moreover, opposite nozzles also contribute to generation of more recirculating vertices formation at the stressing zone by meeting the opposite stream jets at the central point as observed by Huang et al. (2024) in a steam jet mill and Koeninger et al. (2018b) who visualised the similar behaviour experimentally.

The velocity profile gradually decreases while moving away from the stressing zone due to momentum exchange between the continuous phase and the discrete particles. Further it can be observed that high velocity region is found near the apparatus walls as compared to the central region. This effect is even more prominent when air flow is increased from Case 1 to Case 3. For example, the maximum velocity of flow field near the wall at Plane 3 was observed to be 50 m/s for Case 2 which was 12 m/s and 20 m/s in Case 1 and Case 2, respectively (Fig. 9).

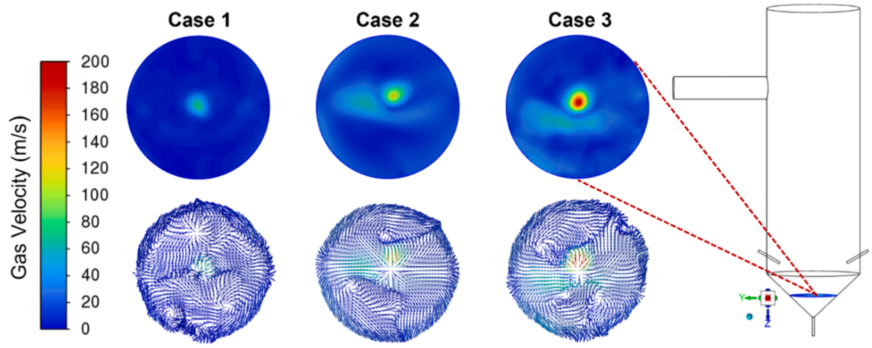

Fig. 7. Comparison of velocity profile at Plane 1 (h: 0.02 m).

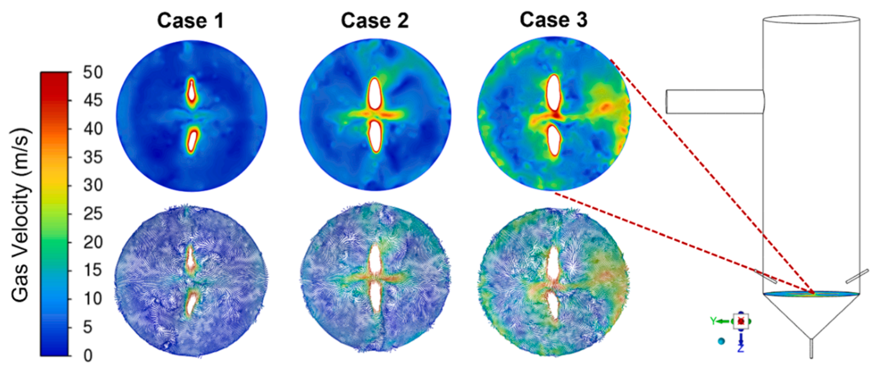

Fig. 8. Comparison of velocity profile at Plane 2 (h: 0.05 m). The white spots indicate the area with high-speed caused by counter jets.

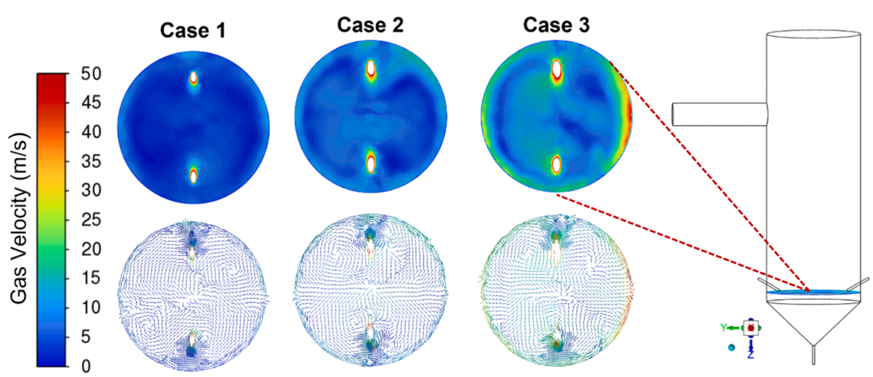

Fig. 9. Comparison of velocity profile at Plane 3 (h: 0.06 m). The white spots indicate the area with high-speed caused by counter jets.

Similarly, the velocity of flow field further decreases due to the decay and dispersion of both phases in the transportation region (Fig. 10).

At Plane 5, the velocity is increased again which is due to the smaller outlet diameter (Fig. 11). Moreover, it should be noted that the outlet boundary was set to restrict the particle movement at the outlet. As a results, particles may accumulate near the outlet region. Due to high gas mass flow, this effect is more prominent in Case 3 (Fig. 11). However, flow vertices can still be observed in the apparatus domain which help to recirculate the particles which again removes these particles and avoid their accumulation (Fig. 11 and Fig. 12).

High particle concentration is observed near the classification wall due to particle cluster formation in the classifier as experimentally observed by Koeninger et al. (2019), significantly affecting the flow dynamics near the classification section as shown in Figs. 11 and 13. Similarly, higher inlet gas velocities are always attractive for particle mixing. However, too high jet velocity cause elutriation of particles in the fluidized bed jet mills which has been visually observed by Kolan et al. (2024). Therefore, optimization of classifier speed with respect to multiphase flow characteristics is also important factor for efficient process outcomes which will be intensively investigated in our further work.

3.3. Effect of injection rate on particle flow

Fig. 13 represents the comparison of particle tracks coloured by the particle velocity magnitude in the whole domain. High velocity of particles is found in the stressing zone where high-speed jet rapidly moves the particles reaching in front of the nozzles and recirculating them towards the mixing zone. The velocity of particles gradually decreases while moving to the upper part of the apparatus. However, fast moving particles can be observed near the outlet section (Fig. 13). As described earlier, this is due to the particle flow restriction and its interaction with counter flow field which carry these particles towards the wall region. The comparison between different air flow rate showed that as expected

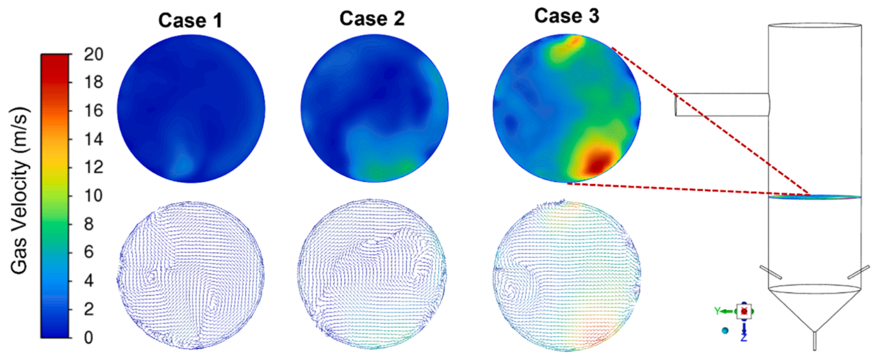

Fig. 10. Comparison of velocity profile at Plane 4 (h: 0.15 m).

the particle velocity also increases with an increase in air flow injected from the inlet nozzles. However, in case of too high air jet injected into the domain (i.e., Case 3), the particles tend to stick more to the apparatus walls rather moving in the central region to improve the particle interaction and overall mixing performance. Hence, it was noted that in Case 3 higher concentration of particles is found near the wall, particularly in the upper region of the fluidized bed which shows less dispersion as compared to the other cases (Fig. 14).

The simulation results hold a good qualitative agreement with the previous findings. For example, Rajeswari et al. (2011) and Santos et al.

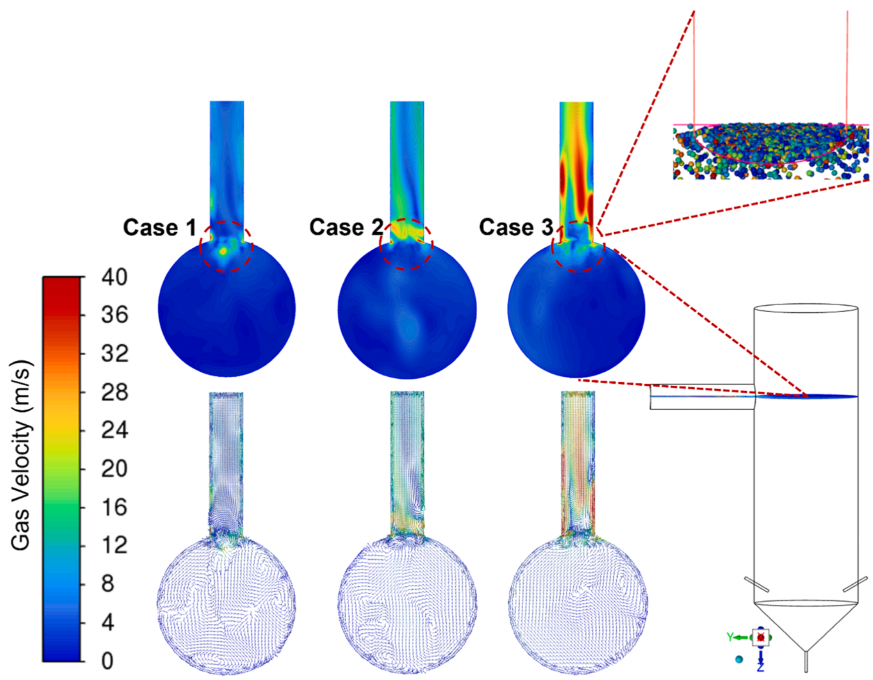

Fig. 11. Comparison of velocity profile at Plane 5 (h: 0.25 m).

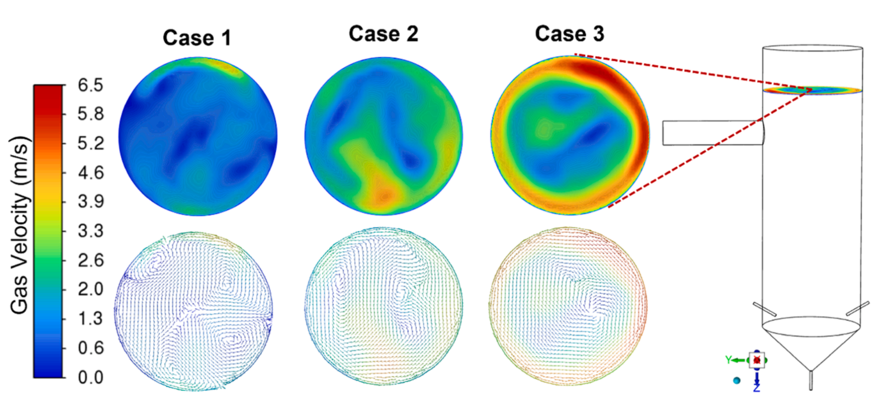

Fig. 12. Comparison of velocity profile at Plane 6 (h: 0.29 m).

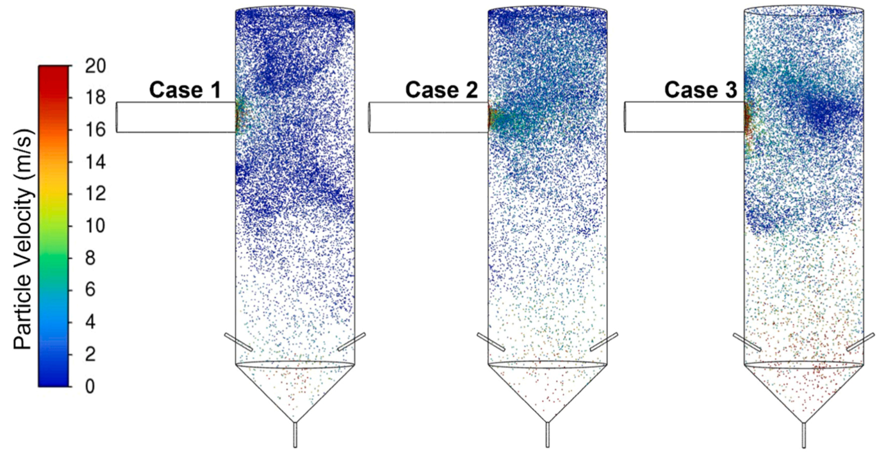

Fig. 13. Comparison of particle tracks coloured by particle velocity magnitude.

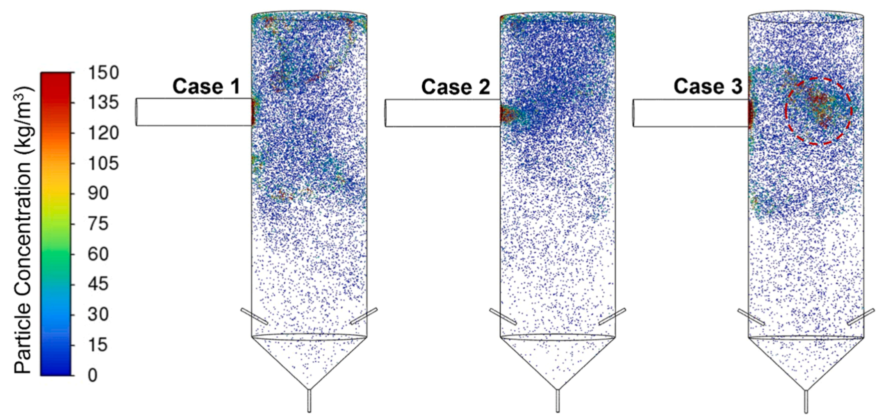

Fig. 14. Comparison of particle tracks coloured by particle concentration.

(2020) found that despite of a high jet injection rates, the velocity of particle phase is much lower than the gas phase velocity in the opposed jets fluidized bed. The corresponding particle and gas velocity was observed as 56 m/s and 508 m/s, respectively in Rajeswari et al. (2011) whereas Santos et al. (2020) reported a particle velocity of 88 m/s with gas velocity of 330 m/s.

The aim of the present study was to systematically investigate hydrodynamics and multiphase mixing in an opposed jets fluidized bed using numerical simulations. Direct experimental measurements in such equipment are extremely challenging due to the presence of high-pressure gas jets, intense particle–particle collisions, and strong turbulence, which make intrusive probes or optical diagnostics difficult to implement and prone to damage or significant measurement uncertainty. In particular, the jet impingement (grinding/mixing) region is highly dynamic and remains poorly characterized experimentally. Furthermore, quantitative experimental data on particle-flow dynamics (e.g., particle concentration, RTD, mixing indices) in opposed jets fluidized beds or jet mills are very scarce in the literature, as most experimental studies focus on milling performance rather than detailed hydrodynamics. The Euler–Lagrange (CFD-DEM) approach employed here has been extensively validated for gas–solid systems such as fluidized and spouted beds, as documented in the cited references. The present work builds on this validated framework to provide new insights into mixing behavior in opposed jets fluidized beds.

In order to further analyse the particle flow and resulting micro-hydrodynamics, the DPM particle data was extracted from ANSYS (Fluent) solutions and processed for the determination of individual particle speed. As illustrated in Fig. 13 and Fig. 14, particles experience

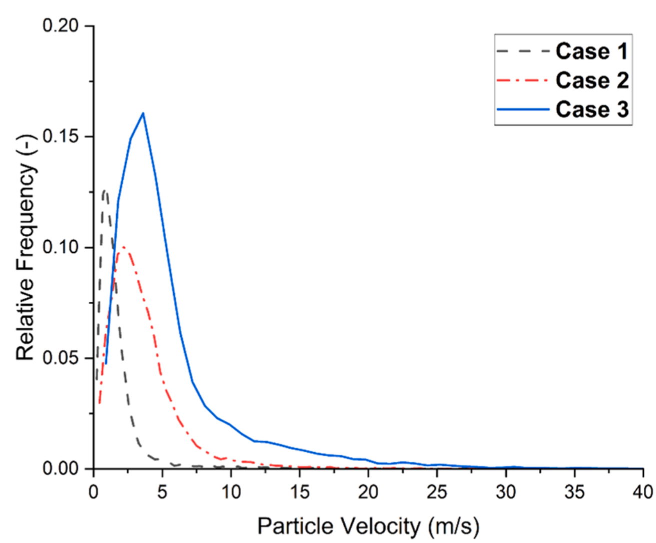

Fig. 15. Comparison of particle velocity distribution with respect to different gas injections.

highly turbulent flows in the stressing zone as a result of high-speed jets. The particles are pushed by the recirculating jets and move towards the upper part of the apparatus with diverse speeds. Fig. 15 illustrates the comparison of particle velocity distribution among the three cases of jet injection. In Case 1, a sharp peak is formed by the high energy particles excited by the injected gas jet. However, the velocity of particles reduces gradually while moving towards the transportation zone resulting in a lower velocity profile as compared to the other two cases. This represents low random movement in the transportation zone in Case 1. Comparatively, a wider distribution with high velocity of particle is observed in Case 2 (Fig. 15). This shows more frequent particle movement and velocity fluctuation in the apparatus. Similarly, the velocity profile curve is more shifted to right by increasing injection jet velocity from Case 2 to Case 3. This represents a wider population of particles possess high speed, eventually leading to a highly random flow in the fluidized bed. Hence, by increasing mass flow rate of gas jet, a higher level of agitation and particle can be achieved in the system (Fig. 15). However, the deposition and layering of particles at the apparatus walls (as shown in Fig. 14) needs to be taken into account for higher gas speeds.

Fluctuating velocity and kinetic agitation of particle are one of the important factors which can be used to describe the particle random movement in comparison with the bulk flow. As result of random movement in the fluid phase, the particles flow with varying speed. Hence, fluctuating velocity can describe how the speed of an individual particle varies with respect to mean velocity of all particles. The fluctuating velocity of particles in each direction is expressed as (Taylor-Noonan et al., 2021; Yu et al., 2020):

$$V_{f,x} = V_x - V_{x\_mean} \tag{12}$$

$$V_{f,y} = V_y - V_{y\_mean} \tag{13}$$

$$V_{f,z} = V_z - V_{z\_mean} \tag{14}$$

where, $V_{f,x}$, $V_{f,y}$ and $V_{f,z}$ are the fluctuating velocities of particle (i) in x, y and z direction which is obtained from the respective particle velocity (V) and mean velocity (V_{mean}) of all particles.

The granular temperature is a measure of kinetic energy, or in other terms, collision potential among the particles moving in the fluidized bed. This can be used to characterize the stressing zone as well as the mixing index of the particles. The granular temperature T_G can be determined based on fluctuating velocities as (Berzi and Jenkins, 2015; Jenkins and Berzi, 2010; Ray and Khakhar, 2023; Taylor-Noonan et al., 2021; Yu et al., 2020):

$$T_G = \frac{1}{3}\left[\left(V_{f,x}\right)^2 + \left(V_{f,y}\right)^2 + \left(V_{f,z}\right)^2\right] \tag{15}$$

Fig. 16 illustrates the granular temperature of particles with respect to the different gas flow rates. It can be observed that a small fraction of the particles represents significantly higher values of granular temperature which causes elongated tail alike curves (Fig. 16). As discussed above, the particles after reflecting back from the outlet and the apparatus wall come across highly turbulent flows from the jet nozzles. Eventually, this significantly increases the particle energy and thus, higher values of granular temperature can be observed. However, after moving towards the mixing zone, the particles dissipate energy which reduces the particle velocity and hence, result in lower values of granular temperature. However, still multiphase interaction and mixing can be expected at the mixing zone because of random movement of particles. The comparison of the three cases showed that increasing jet inlet velocity, a significant energy is induced in the stressing zone which increases the granular temperature of the particles. For example, Case 3 shows an inclined curve which implies more particles have higher values of kinetic energy as compared to the other two cases. The average granular temperature of all particles has been observed as 3.24 m^2/s^2, 7.41 m^2/s^2 and 20.38 m^2/s^2 for Case 1, Case 2 and Case 3, respectively. Particle fluctuating velocity is considerably increased due to more randomized movement of particles as compared to the mean flow and hence, more energy in particles is observed in Case 3.

The findings of current numerical simulations are helpful to identify

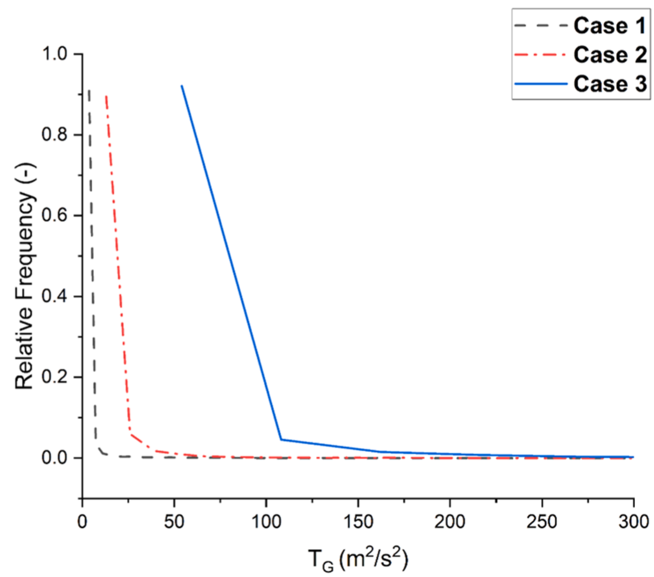

Fig. 16. Comparison of particle granular temperature with respect to different gas injections.

the regions of dominant flow regimes and vertices at different locations within the apparatus. The behavior and pathways of particles under variable injections can be used to decide the upper limit of gas injection rates without formulation of wall bounded ring. Hence, the information obtained from current study is useful for the process optimization of micron sized particles in opposed jets fluidized beds.

4. Conclusions

A two-way coupled Euler-Lagrange based numerical approach has been employed to investigate internal hydrodynamics of an opposed jets fluidized bed. Mixing of 20000 fine aggregates was studied under different operating conditions. The main conclusions are summarized as: 1) Typical opposed jet nozzles exhibit counter flow pattern which causes recirculation vertices in the stressing zone. Eventually, the bottom jet experiences this strong counter flow that deviates its flow path and hence, vertices are further enhanced. 2) The particle dispersion and mixing are significantly enhanced by increasing air flow rate leading to high kinetic energy of particles. Maximum particle velocity was observed as 47 m/s, 88 m/s and 180 m/s with the gas injections at a rate of 0.001 kg/s, 0.002 kg/s and 0.003 kg/s, respectively. 3) Too high air jet (i.e. Case 3) pushes the particles towards the apparatus wall in the mixing zone and hence, reduces the interaction in the upper region. Consequently, the particles intend to stick to the apparatus wall through ring formulation. A wall bounded ring with particle concentration of 150 kg/m^3 was found in Case 3 at the apparatus wall near the outlet. These findings contribute to a foundational understanding of multiphase flow and mixing of micron sized particles in opposed jet fluidized beds. Further studies are planned to investigate particle collisions, dynamic effect of classifier, variable particle sizes and mass loadings.

CRediT authorship contribution statement

Dyrney Araújo dos Santos: Writing – review & editing, Investigation. **Andreas Bück:** Writing – review & editing, Supervision, Resources, Project administration, Methodology, Funding acquisition, Conceptualization. **Laura Unger:** Methodology, Investigation, Conceptualization. **Muhammad Usman Farid:** Writing – original draft, Software, Investigation, Formal analysis.

Declaration of Competing Interest

The authors declare that they have no known competing financial interests or personal relationships that could have appeared to influence the work reported in this paper.

Acknowledgements

The authors gratefully acknowledge the funding of this work provided by Deutsche Forschungsgemeinschaft (DFG) in the framework of Priority Programme 2289 'Hetero-Aggregates' (Project ID 462314498 (Bück, Schmidt)).

Data Availability

Data will be made available upon request to the corresponding author.

References

Ali, S.S., Asif, M., 2017. Effect of particle mixing on the hydrodynamics of fluidized bed of nanoparticles. Powder Technol. 310, 234–240. https://doi.org/10.1016/j.powtec.2017.01.041.

Berzi, D., Jenkins, J.T., 2015. Steady shearing flows of deformable, inelastic spheres. Soft Matter 11 (24), 4799–4808. https://doi.org/10.1039/C5SM00337G.

Chen, K., Bachmann, P., Bück, A., Jacob, M., Tsotsas, E., 2019. CFD simulation of particle residence time distribution in industrial scale horizontal fluidized bed. Powder Technol. 345, 129–139. https://doi.org/10.1016/j.powtec.2018.12.086.

Dennis, S., Singh, S., Ingham, D., 1980. The steady flow due to a rotating sphere at low and moderate Reynolds numbers. J. Fluid Mech. 101 (2), 257–279. https://doi.org/10.1017/S0022112080001656.

Farid, M.U., Bück, A., Heineken, W., Gohla, M., Zobel, N., 2017. Study on nozzle design for combustion of solid materials with low melting points. Appl. Therm. Eng. 115, 832–859. https://doi.org/10.1016/j.applthermaleng.2017.01.006.

Farid, M.U., Olbert, I.A., Bück, A., Ghafoor, A., Wu, G., 2025. CFD modelling and simulation of anaerobic digestion reactors for energy generation from organic wastes: a comprehensive review. Heliyon 11, e41911. https://doi.org/10.1016/j.heliyon.2025.e41911.

Fluent, A., 2022. Ansys Theory Guide. In: ANSYS, R2. ANSYS Inc.. ⟨www.ansys.com⟩

Gao, W., Chen, F., Wang, X., Meng, Q., 2020. Recent advances in processing food powders by using superfine grinding techniques: a review. Compr. Rev. Food Sci. Food Saf. 19 (4), 2222–2255. https://doi.org/10.1111/1541-4337.12580.

Ghoroi, C., Han, X., To, D., Jallo, L., Gurumurthy, L., Davé, R.N., 2013. Dispersion of fine and ultrafine powders through surface modification and rapid expansion. Chem. Eng. Sci. 85, 11–24. https://doi.org/10.1016/j.ces.2012.02.038.

Huang, S., Zhang, Y., Yin, X., Zhang, M., Li, H., Wang, Z., Chen, H., Wang, H., 2024. Effect of nozzle quantity on the flow field characteristics and grinding efficiency in a steam jet mill. Processes 12 (7), 1500. https://doi.org/10.3390/pr12071500.

Jadidi, B., Ebrahimi, M., Ein-Mozaffari, F., Lohi, A., Neveu, A., Francqui, F., 2025. Analysis of cohesive mannitol particle mixing: a comparative study of machine learning methods. Chem. Eng. Res. Des. 214, 188–201. https://doi.org/10.1016/j.cherd.2024.12.040.

Jenkins, J.T., Berzi, D., 2010. Dense inclined flows of inelastic spheres: tests of an extension of kinetic theory. Granul. Matter 12 (2), 151–158. https://doi.org/10.1007/s10035-010-0169-8.

Koeninger, B., Hensler, T., Romeis, S., Peukert, W., Wirth, K.-E., 2018a. Dynamics of fine grinding in a fluidized bed opposed jet mill. Powder Technol. 327, 346–357. https://doi.org/10.1016/j.powtec.2017.12.084.

Koeninger, B., Koegl, T., Hensler, T., Arlt, W., Wirth, K.-E., 2018b. Solid distribution in fluidized and fixed beds with horizontal high speed gas jets. Powder Technol. 336, 57–69. https://doi.org/10.1016/j.powtec.2018.05.035.

Koeninger, B., Spoetter, C., Romeis, S., Weber, A.P., Wirth, K.-E., 2019. Classifier performance during dynamic fine grinding in fluidized bed opposed jet mills. Adv. Powder Technol. 30 (8), 1678–1686. https://doi.org/10.1016/j.apt.2019.05.018.

Kolan, S.R., Wang, R., Hoffmann, T., Tsotsas, E., 2024. Mixing nanoparticles in a ProCell type spouted bed. Powder Technol. 431, 119129. https://doi.org/10.1016/j.powtec.2023.119129.

Lee, H.W., Song, S., Kim, H.T., 2019. Improvement of pulverization efficiency for micro-sized particles grinding by uncooled high-temperature air jet mill using a computational simulation. Chem. Eng. Sci. 207, 1140–1147. https://doi.org/10.1016/j.ces.2019.07.025.

Lepek, D., Valverde, J.M., Pfeffer, R., Dave, R.N., 2010. Enhanced nanofluidization by alternating electric fields. AIChE J. 56 (1), 54–65. https://doi.org/10.1002/aic.11954.

Lince, F., Marchisio, D.L., Barresi, A.A., 2011. A comparative study for nanoparticle production with passive mixers via solvent-displacement: use of CFD models for optimization and design. Chem. Eng. Process. Process.Intensif. 50 (4), 356–368. https://doi.org/10.1016/j.cep.2011.02.015.

Liu, H., Wang, S., 2021. Fluidization behaviors of nanoparticle agglomerates with high initial bed heights. Powder Technol. 388, 122–128. https://doi.org/10.1016/j.powtec.2021.04.088.

Lu, J., Guo, Y., Xin, Y., Yang, X., Li, J., 2025. Turbulence-assisted shear regulatable synthesis of Ag nanoparticles using a counter axial-swirling impinging jet flow reactor. Chem. Eng. Sci., 121418 https://doi.org/10.1016/j.ces.2025.121418.

Men, J., Kolan, S.R., Massomi, A., Hoffmann, T., Schmidt, J., Tsotsas, E., Bück, A., 2023. Formulation of nanostructured heteroaggregates by fluidization technologies. Chem. Ing. Tech. 95 (1-2), 107–113. https://doi.org/10.1002/cite.202200139.

Menter, F.R., Kuntz, M., Langtry, R., 2003. Ten years of industrial experience with the SST turbulence model. Turbul. Heat. Mass Transf. 4 (1), 625–632.

Nascimento, R.F., Men, J., Düsenberg, B., Schmidt, J., Bück, A., 2025. Formulation of hetero-aggregates in opposed jet fluidized beds. Powder Technol. 461, 121099. https://doi.org/10.1016/j.powtec.2025.121099.

Peukert, W., Bück, A., 2024. Green" particle technology: its history, successes, and open issues. Powder Technol. 448, 120255. https://doi.org/10.1016/j.powtec.2024.120255.

Quevedo, J.A., Omosebi, A., Pfeffer, R., 2010. Fluidization enhancement of agglomerates of metal oxide nanopowders by microjets. AIChE J. 56 (6), 1456–1468. https://doi.org/10.1002/aic.12075.

Rajeswari, M.S.R., Azizli, K., Hashim, S., Abdullah, M., Mujeebu, M.A., Abdullah, M., 2011. CFD simulation and experimental analysis of flow dynamics and grinding performance of opposed fluidized bed air jet mill. Int. J. Miner. Process. 98 (1-2), 94–105. https://doi.org/10.1016/j.minpro.2010.10.012.

Ray, N.S., Khakhar, D., 2023. A method for coarse graining fluctuation velocities in granular flows. Granul. Matter 25 (3), 46. https://doi.org/10.1007/s10035-023-01338-7.

Salloum, N., Brinz, T., Atxutegi, A., Heinrich, S., 2025. Design and optimization of stirrer and mixer design for the correct mixing of pharmaceutical powders through DEM. Powder Technol. 449, 120413. https://doi.org/10.1016/j.powtec.2024.120413.

Santos, D.A., Baluni, S., Bück, A., 2020. Eulerian multiphase simulation of the particle dynamics in a fluidized bed opposed gas jet mill. Processes 8 (12), 1621. https://doi.org/10.3390/pr8121621.

Sharma, A., Chakraborty, J., Tripathi, A., Kumar, J., Sen, M., Ketterhagen, W., 2025. Impact of equipment material and surface finish on the flowability of dry cohesive powders–an important consideration in calibration of discrete element models. J. Pharm. Innov. 20 (2), 74. https://doi.org/10.1007/s12247-025-09950-1.

Strobel, A., Köninger, B., Romeis, S., Schott, F., Wirth, K.-E., Peukert, W., 2020. Assessing stress conditions and impact velocities in fluidized bed opposed jet mills. Particuology 53, 12–22. https://doi.org/10.1016/j.partic.2020.02.006.

Sudsuansee, T., Phitaksurachai, S., Pan-Aram, R., Sritrakul, N., Tiaple, Y., 2025. Design and hydrodynamic performance of low head propeller hydro turbine for wide range high efficiency operation. Int. J. Thermofluids, 101228. https://doi.org/10.1016/j.ijft.2025.101228.

Tashakori-Asfestani, F., Kazemi, S., Zarghami, R., Mostoufi, N., 2023. Effect of inter-particle forces on solids mixing in fluidized beds. Powder Technol. 415, 118098. https://doi.org/10.1016/j.powtec.2022.118098.

Taylor-Noonan, A.M., Gollin, D., Bowman, E.T., Take, W.A., 2021. The influence of image analysis methodology on the calculation of granular temperature for granular flows. Granul. Matter 23 (4), 96. https://doi.org/10.1007/s10035-021-01153-y.

Thomas, A.L., 2025. A mechanistic framework for the characterisation of cohesive, frictional and interlocking effects on powder flow behaviour. Particuology 101, 90–106. https://doi.org/10.1016/j.partic.2024.01.003.

Unger, L., Gómez Bonilla, J.S., Santos, D.A., Bück, A., 2022. Particle residence time distribution in a concurrent multiphase flow reactor: Experiments and Euler-Lagrange simulations. Processes 10 (5), 996. https://doi.org/10.3390/pr10050996.

Van Ommen, J.R., Valverde, J.M., Pfeffer, R., 2012. Fluidization of nanopowders: a review. J. Nanopart. Res. 14, 1–29. https://doi.org/10.1007/s11051-012-0737-4.

Wróblewski, A., Macek, A., Bansiewicz, A., Wodecki, J., 2024. Comparison of Hexcore and Poly-Hexcore computational meshes in the aspect of air flow modeling based on the actual geometry of mining excavations. IOP Conf. Series Earth Environ. Science 1295, 012007. https://doi.org/10.1088/1755-1315/1295/1/012007.

Yu, Y., Zhao, L., Li, Y., Zhou, Q., 2020. A Model to Improve Granular Temperature in CFD-DEM simulations. Energies 13 (18), 4730. https://doi.org/10.3390/en13184730.